JGR Solid Earth

RESEARCH ARTICLE
10.1029/2023JB027680

Thousand-Kilometer DAS Array Reveals an Uncatalogued Magnitude-5 Dynamically Triggered Event After the 2023 Turkey Earthquake

Qiushi Zhai[1], **Zhongwen Zhan**[1], **and J. Andres Chavarria**[2]

[1]Seismological Laboratory, California Institute of Technology, Pasadena, CA, USA, [2]LUNA-OptaSense, Chino, CA, USA

Key Points:

- We find an uncatalogued M5.1 earthquake in NE Turkey dynamically and instantaneously triggered by the 2023 Mw 7.8 SE Turkey earthquake
- We uncover this event on a thousand-kilometer linear distributed acoustic sensing array, then confirm its precise time, location, and magnitude with seismometers
- Precursory signals of the M5.1 event are observed and are most likely resulting from other nearby events rather than its nucleation phase

Supporting Information:

Supporting Information may be found in the online version of this article.

Correspondence to:

Q. Zhai,
qzhai@caltech.edu

Citation:

Zhai, Q., Zhan, Z., & Chavarria, J. A. (2024). Thousand-kilometer DAS array reveals an uncatalogued magnitude-5 dynamically triggered event after the 2023 Turkey earthquake. *Journal of Geophysical Research: Solid Earth*, *129*, e2023JB027680. https://doi.org/10.1029/2023JB027680

Received 14 AUG 2023
Accepted 16 FEB 2024

Author Contributions:

Conceptualization: Qiushi Zhai, Zhongwen Zhan
Data curation: J. Andres Chavarria
Formal analysis: Qiushi Zhai
Funding acquisition: Zhongwen Zhan
Investigation: Qiushi Zhai
Methodology: Qiushi Zhai
Resources: Zhongwen Zhan
Supervision: Zhongwen Zhan, J. Andres Chavarria
Writing – original draft: Qiushi Zhai
Writing – review & editing: Qiushi Zhai, Zhongwen Zhan, J. Andres Chavarria

Abstract Large earthquakes can trigger smaller seismic events, even at significant distances. The process of earthquake triggering offers valuable insights into the evolution of local stress states, deepening our understanding of the mechanisms of earthquake nucleation. However, our ability to detect these triggered events is limited by the quality and spatial density of local seismometers, posing significant challenges if the triggered event is hidden in the signal of a nearby larger earthquake. Distributed acoustic sensing (DAS) has the potential to enhance the monitoring capability of triggered earthquakes through its high spatial sampling and large spatial coverage. Here, we report on an uncatalogued magnitude (M) 5.1 event in northeast Turkey, which was likely dynamically and instantaneously triggered by the 2023 M7.8 earthquake in southeast Turkey, located 400 km away. This event was initially discovered on ~1,100 km of active DAS recordings that are part of an 1,850-km linear array. Subsequent validation using local seismometers confirmed the event's precise time, location, and magnitude. Interestingly, this dynamically triggered event exhibited precursory signals preceding its P arrivals on the nearby seismometers. It can be interpreted as the signal from other nearby, uncatalogued, smaller triggered events. Our results highlight the potential of high-spatial-density DAS in enhancing the local-scale detection and the detailed analysis of earthquake triggering.

Plain Language Summary Large earthquakes can trigger smaller ones even far away. This helps us understand more about how earthquakes start and develop. However, finding these smaller earthquakes can be difficult as sometimes they are hidden in the chaos of a bigger, nearby earthquake. There is a novel technology called Distributed Acoustic Sensing (DAS) that might help. DAS can listen for earthquakes over large areas and gives a more detailed picture of what's happening underground. In this study, we discovered a moderate-size earthquake with a magnitude of 5.1 in Northeast Turkey that was triggered by a large earthquake with a magnitude of 7.8 in Southeast Turkey, using a DAS system that stretched over a thousand kilometers. We then checked this finding with conventional seismometers to be sure. Interestingly, this triggered earthquake showed precursory signals before its main shaking started, which could be signs of other smaller earthquakes happening nearby. Our findings deepen our understanding of how earthquakes interact with each other and offer insights into how earthquakes start. Our results also suggest that DAS could help us find and understand these triggered earthquakes, providing us with invaluable information for future seismology studies.

1. Introduction

Stress changes related to an earthquake are capable of triggering other earthquakes both in adjacent areas and at long-range distances (Freed, 2005). In the past three decades, earthquake triggering at large distances outside the regional fault network of the mainshock has been documented in various tectonic settings (Aiken & Peng, 2014; Hill & Prejean, 2015). For example, the dynamically triggered seismicity following the 1992 M7.3 Landers earthquake (Hill et al., 1993), the 1999 M7.4 Turkey earthquake (Brodsky et al., 2000), the 2002 M7.9 Denali Fault earthquake (Prejean et al., 2004), the 2010 M8.8 Chile earthquake (C. Li et al., 2021; Peng et al., 2010), the 2016 M7.3 Kumamoto earthquake (Kato et al., 2016), and the 2016 M7.8 Kaikoura earthquake (Yao et al., 2021). The triggering process is commonly explained with the Coulomb failure criterion, which states that an earthquake is triggered when the combined external static or dynamic stress and the in-situ shear stress acting on a near-failing fault exceed the fault's strength (Jaeger et al., 2009; Scholz, 2019). If a seismic event occurs within the time window when transient seismic signals (e.g., P, S, or surface waves) surpass the background noise level at that location, this phenomenon is called instantaneous triggering (Antonioli et al., 2006; Tape et al., 2013).

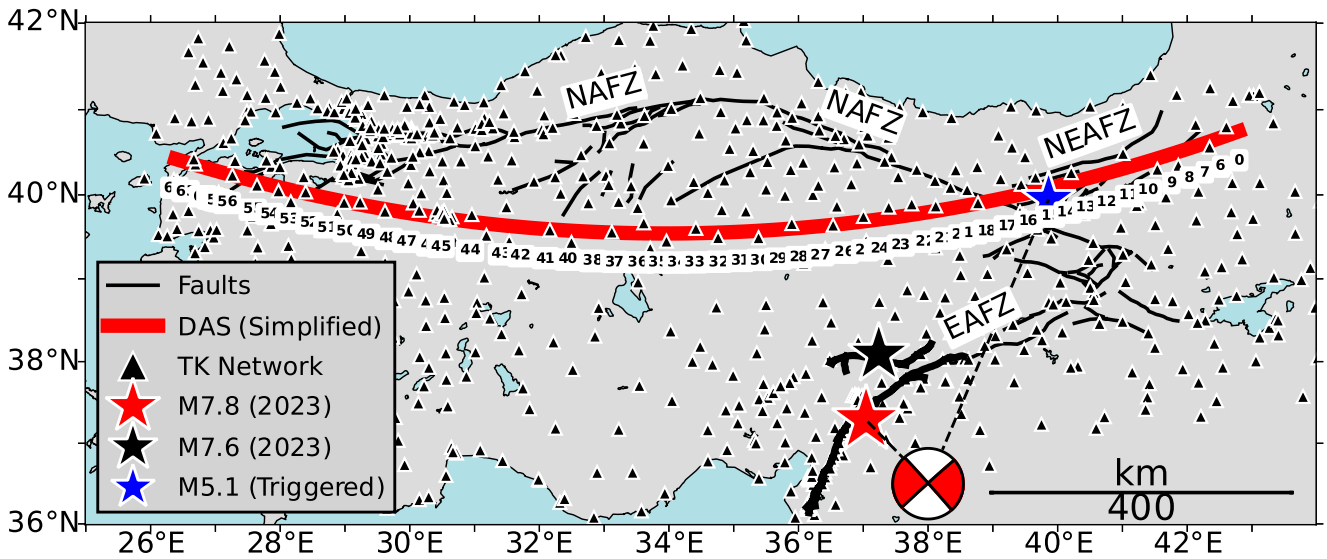

Figure 1. The map of the study region. The red star represents the M7.8 mainshock. The blue star represents the M5.1 earthquake, occurring shortly after the M7.8 mainshock, as detected by multiple DAS arrays/segments covering ~1,100 km of fiber (simplified red line with the index of segments under it). Thick black lines are the fault rupture mapping of the M7.8 and M7.6 events (Reitman et al., 2023). EAFZ: East Anatolian Fault Zone, NAFZ: North Anatolian Fault Zone, NEAFZ: Northeast Anatolian Fault Zone (Bozkurt, 2001; Irmak et al., 2012; Şengör et al., 1985). Note the precise locations of the DAS channels have been intentionally blurred due to security concerns.

Earthquake triggering can be used to infer the stresses required for failure and the stress state on faults at depth (Brodsky & van der Elst, 2014). It can also provide insights into the physics of earthquake nucleation (Tape et al., 2013). Despite advancements in data mining techniques, such as back-projection (Fan & Shearer, 2016; Ishii et al., 2005), template matching (Gibbons & Ringdal, 2006; Shelly et al., 2007; Zhai et al., 2021, 2023), and machine learning (Tang et al., 2020; Zhu & Beroza, 2018), the capacity to effectively monitor earthquake triggering remains constrained by the quality and quantity of local seismometers. For example, Liu et al. (2017) only had access to a single high-quality seismometer, significantly impeding the precise determination of the location and magnitude of the triggered events in their target region.

Distributed acoustic sensing (DAS) is emerging as a transformative tool in seismic monitoring (Parker et al., 2014). One DAS interrogator can convert up to one hundred kilometers of optical fiber into a dense array of strainmeters with a few meters of sensor spacing (Lindsey & Martin, 2021; Zhan, 2019). The interrogator sends repeated laser pulses into an optical fiber and measures the Rayleigh back-scattering from the fiber's inherent heterogeneities. By calculating the phase changes in the backscattering using optical interferometry, DAS can infer the strain or strain rate along either a pre-existing telecommunication or a dedicated fiber cable. Recent studies have proven the efficacy of DAS in capturing seismic signals across a broad frequency band (Lindsey et al., 2020; Paitz et al., 2021) in diverse environments, such as terrestrial (Lindsey et al., 2017), submarine (Williams et al., 2019), and glacial settings (Walter et al., 2020). This has considerably advanced seismological studies, enhancing our understanding of seismic sources and earth structure (Ajo-Franklin et al., 2019; J. Li, Kim, et al., 2023; J. Li, Zhu, et al., 2023; Lindsey et al., 2019; Martin et al., 2017; Nayak et al., 2021; Spica et al., 2020). As for earthquake triggering, borehole DAS has proven instrumental in monitoring hydraulic fracturing activities and induced seismicity in the energy industry (Chavarria et al., 2022; Karrenbach et al., 2017; Mateeva et al., 2014; Molenaar et al., 2011). With the rapid deployment of a DAS operating from 4 days post-mainshock, Z. F. Li et al. (2021) detected six times more aftershocks than the standard catalog, surrounding the 2019 M7.1 Ridgecrest earthquake. However, there is limited documentation on using DAS to detect seismic events instantaneously triggered by the passing seismic wave of distant, large earthquakes.

Using DAS, this study presents the discovery and analysis of an earthquake in NE Turkey dynamically triggered by the 2023 M7.8 earthquake 400 km away in SE Turkey (Figure 1). This triggered event is special for the following reasons: (a) It is an instantaneously and dynamically triggered M5 event that was uncatalogued by any standard catalog. (b) The ~1,100-km-long active array (Figure 1), which is part of the longest (1,850 km)

operating DAS system to our best knowledge, provides a unique contribution to the discovery of this event. Otherwise, analysts could likely miss this M5 event if only using conventional seismic sensors. (c) This event exhibited exponential precursory signals preceding its P arrivals on the two closest stations at 14 and 22 km. This signal can be interpreted as other nearby, uncatalogued, smaller triggered events. In the following sections, we present the DAS recordings of the M7.8 mainshock and the discovery of the M5.1 triggered event. We then verify it on the local conventional seismometers, measuring its accurate time, location, and magnitude. We will conclude with a discussion on the triggering mechanism of this event and the signal preceding its P arrivals.

2. Two M7 SE Turkey Earthquakes on the Thousand-Kilometer DAS Data

On 6 February 2023, at 01:17 UTC, a moment magnitude (Mw) 7.8 earthquake struck southeastern Turkey and northwestern Syria. Based on the Disaster and Emergency Management Authority of Turkey (AFAD) earthquake catalog (Kadirioğlu et al., 2018), this mainshock triggered an Mw 6.6 aftershock 10 min after it, and more than 10 Mw > 5 aftershocks in the following few hours. Furthermore, an Mw 7.6 earthquake occurred approximately 90 km northwest of the Mw 7.8 event just 9 hr later (Figure 1). This Mw 7.6 earthquake was likely promoted by the static stress changes induced by the Mw 7.8 earthquake slips (Toda et al., 2023).

Seismic and geodetic data analysis (Barbot et al., 2023; Dal Zilio & Ampuero, 2023; Delouis et al., 2023; Jia et al., 2023; Mai et al., 2023; Melgar et al., 2023; Meng et al., 2024; Okuwaki et al., 2023; Reitman et al., 2023; Ren et al., 2024) reveal that the Mw 7.8 mainshock achieved a peak slip of around 8–12 m, rupturing for over 100 s along 350 km segments of the East Anatolian Fault Zone (EAFZ) (Figure 1). The subsequent Mw 7.6 earthquake ruptured a 150 km segment on an EAFZ splay fault (Duman & Emre, 2013). The EAFZ is a 700-km left-lateral strike-slip fault accommodating the tectonic movement between the Arabian and Anatolian plates (DeMets et al., 1990). It is the second-largest fault zone in Turkey, following the 1,200-km-long North Anatolian Fault Zone (NAFZ) (Ambraseys, 1970).

Since 2018, 65 OptaSense DAS units (Figure 1) have been operating along a fiber-optic cable that stretches across northern Turkey, spanning from the Georgia-Turkey border in the east to the Greek-Turkish border in the west. These 65 DAS segments, which connect consecutively, create a spatially continuous DAS system close to two thousand kilometers long. While data from some DAS segments were unavailable during the two M7 earthquakes, the remaining segments, extending over 1,100 km, successfully recorded the signals from both earthquakes (Figure 2). The maximum channel spacing is 10 m, which means that this is a dense seismic array consisting of over 110,000 channels/sensors. Although there is some variation in the setup of these DAS segments, the sampling rate never drops below 500 Hz. It's noteworthy that it is an intensity-based DAS system without accurate phase information.

We take several steps to preprocess the raw DAS data. First, we resample the channels in 10-m spacing and resample the waveform in 125 Hz. Next, we take the first derivative of the waveform and then normalize each trace by its peak absolute value. Finally, we correct relative clock inconsistencies between adjacent DAS segments based on their waveform cross-correlation, and address the absolute clock issue by comparison with co-located conventional seismometers. Figure 2 shows the preprocessed data with data gaps on some DAS segments. Figures S1 and S2 in Supporting Information S1 show the data without data gaps plotted. The P and S wave arrival times align approximately with those predicted by a local 1D velocity model (Table S1 in Supporting Information S1) (Melgar et al., 2020).

3. The M5 Uncatalogued Event Following the Mw 7.8 Mainshock

The time-distance patterns for the two M7 earthquakes in Figure 2 are similar because both events are located more than 190 km from the DAS array. However, the DAS recording of the Mw 7.8 earthquake reveals a distinct short-duration signal about 120s after the mainshock on DAS segments #13–#16 (Figure 1) spanning 150 km. Given that its curvature is greater than the P and S phases of the M7 events, this signal must be from a source much closer than the M7 events which are 400 km away from these DAS segments. Therefore, we interpret this signal as a local earthquake. Considering the strong, 150-km-wide signal it superimposes on the background signal from the Mw 7.8 mainshock, we estimate it to be a moderate-magnitude event rather than a microearthquake. However, as of our writing, no events were reported in the 300 s immediately following the Mw 7.8 mainshock in this region in either the local AFAD earthquake catalog or the global ISC and USGS catalogs.

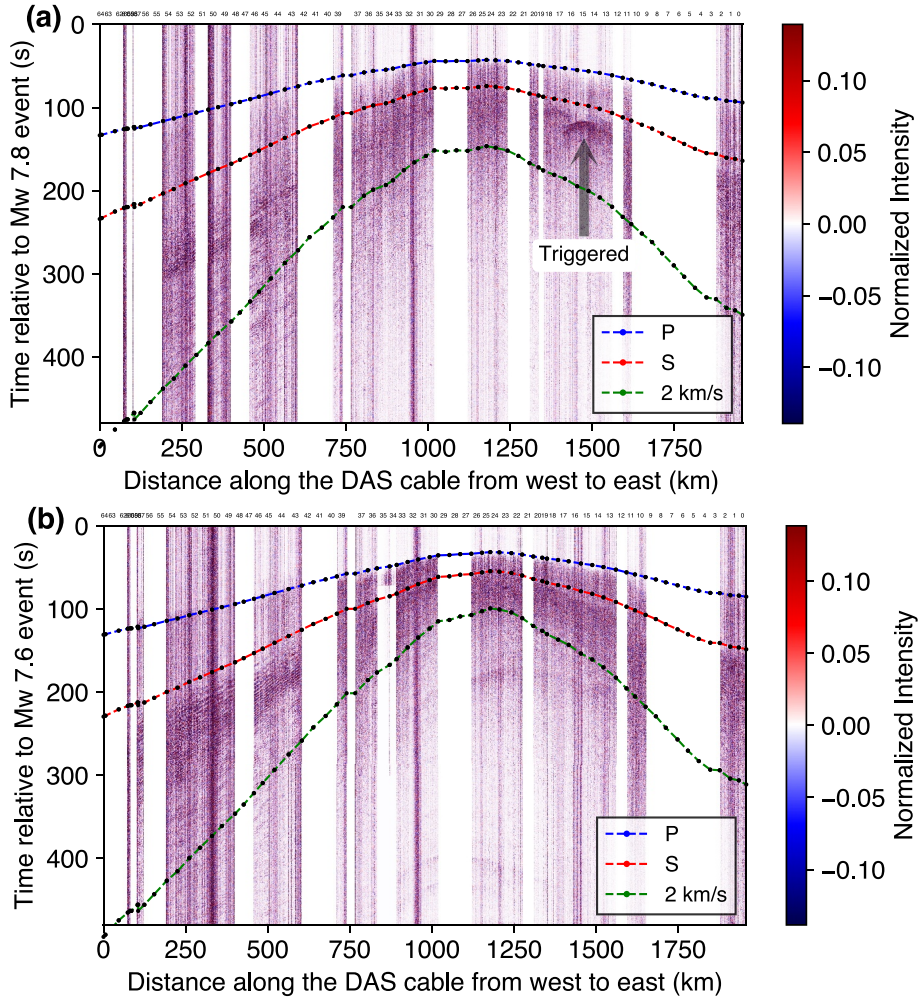

Figure 2. DAS recordings of the Mw 7.8 (a) and Mw 7.6 (b) SE Turkey Earthquakes. The P and S arrival times are predicted based on a local 1D velocity model (Melgar et al., 2020) (Table S1 in Supporting Information S1). The numbers on the top are the index of the DAS segments (Figure 1). The signal of the uncatalogued event is indicated by the gray arrow in (a).

The absence of any large earthquakes (M4.5+) close to this time in the standard catalogs, despite the high density of local conventional seismometers (Figure 1), was unexpected. However, it is reasonable because it occurred only 120s after a much larger (M7.8) mainshock which ruptured over 100s, and the mainshock signal dominates the local seismic recordings and increases the magnitude of completeness (Helmstetter et al., 2006). In the following subsections, we validate the existence of this uncatalogued event by carefully analyzing data from both DAS and local seismometers. This analysis enables us to measure its time, location, and magnitude, and also to investigate potential triggering mechanisms.

3.1. Time and Location

We determine the time and location of the uncatalogued event based on phase arrival times from both DAS and conventional seismometers. First, we use PhaseNet-DAS (Zhu et al., 2023), a machine-learning phase picker for DAS data, to measure the P-wave arrival times. We limit our measurement to DAS segment #15, which exhibits the earliest first arrivals meaning closest to the source, to minimize the effect of clock inconsistencies across independent DAS segments. The P-wave first arrivals are easily picked on this DAS segment because the arrivals are clear (see the sharp color contract in Figure 3). These automatically picked arrivals on DAS are then manually double-checked. Next, we manually pick the first arrivals of P and S waves on the 14 nearby seismometers located 14–166 km away. To minimize the effects of the low-frequency signals from the Mw 7.8 earthquake, manual picking is performed on the high-frequency (>5 Hz) filtered seismometer data (Figure 4). As the Mw 7.8

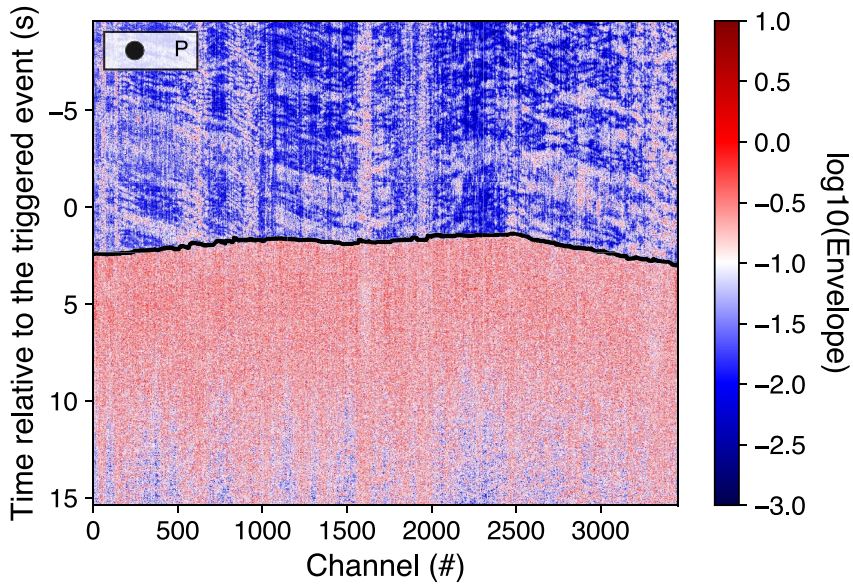

Figure 3. Recordings of the uncatalogued event on the closest DAS segment (#15). The data is optimally visualized via a logarithmically scaled of the waveform's envelope. Black dots represent the P arrivals picked using the PhaseNet-DAS.

earthquake's high-frequency signal is negligible due to long-distance attenuation, this filtering focuses attention on the local event. We then use the NonLinLoc package (Lomax et al., 2000, 2014) with a local 1D velocity model (Melgar et al., 2020) to locate the event, utilizing these phase arrivals from both DAS and seismometers. Figure 5 shows the optimal hypocenter of the uncatalogued event (Latitude: 39.947°, Longitude: 39.860°, Depth: 8.02 km, 392 km away from the Mw 7.8 mainshock). With a root mean square travel time misfit of 0.22s, the location error is approximately 1 km. The time of the optimal hypocenter is 20230206T01:19:36.9678 UTC, occurring 121.17 s after the Mw 7.8 mainshock. This time is within the time window of the high-amplitude S and surface waves. The S wave and surface wave overlap with each other at this location because the Mw 7.8 mainshock is only 400 km away and ruptured for over 100 s.

3.2. Magnitude

The local magnitude of the uncatalogued event is estimated using a regression analysis that leverages the statistical correlations between observed peak amplitudes on seismometers and their respective epicentral distances. The scaling relation aligns with the principles used in a Wood-Anderson seismograph (Richter, 1935):

$$M = \log_{10} A + a \log_{10} \Delta + b \quad (1)$$

where M is the local magnitude, A is the highest peak ground acceleration (PGA) among three components of the strong-motion sensors at epicentral distance Δ. We bandpass filter (2–50 Hz) the data (Figures S3 and S4 in Supporting Information S1) to eliminate the influence of the low-frequency signals from the Mw 7.8 earthquake when measuring this uncatalogued event's PGA. Empirical parameters a and b are determined from the least squares fit of the PGA, distance, and magnitude of the eight cataloged events with a moment magnitude greater than 4 within 0.5 degrees of the uncatalogued event, as per the recent 10-year AFAD catalog. With these fixed parameters ($a = 1.85$ and $b = 1.11$), we calculate the uncatalogued event's magnitude to be 5.1 ± 0.2 by taking the mean and standard deviation of magnitudes measured on all the strong motion stations within a 90 km radius, as outlined in Equation 1.

The amplitude-distance distribution of the uncatalogued event, exhibited in Figure 6, follows a linear pattern in the logarithmic scale. This linearity not only enables us to measure the magnitude but also confirms the robustness of our results of detecting and locating this uncatalogued event. In the absence of such a pattern, the signals we picked could erroneously belong to the Mw 7.8 earthquake. While we utilize only seismometer data in this

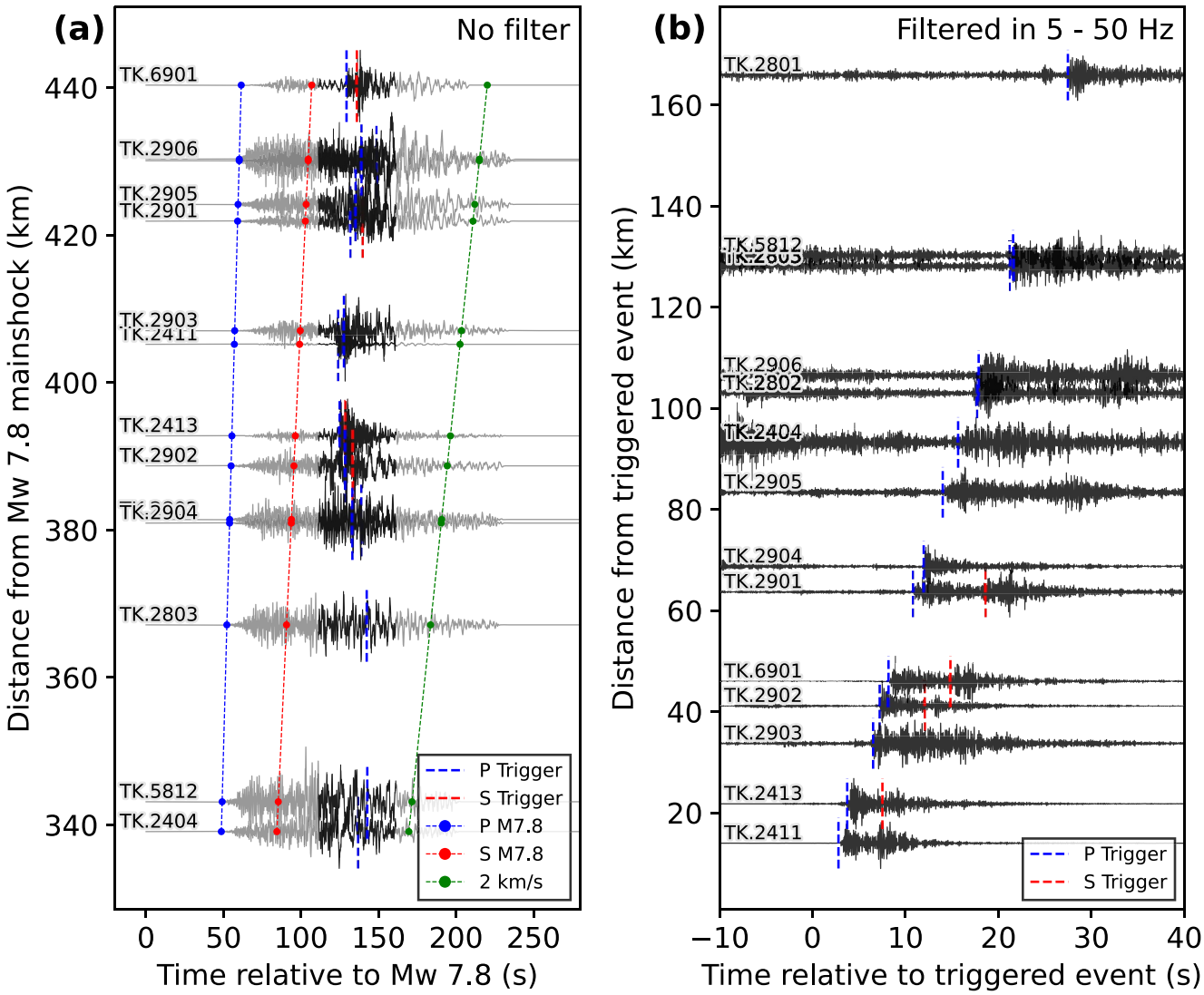

Figure 4. Waveforms of the uncatalogued event on the nearby strong-motion stations. (a) Waveforms of stations near the uncatalogued event, starting from 20 s before the origin time of the Mw 7.8 mainshock, sorted by the distance from the Mw 7.8 mainshock. The darker 50-s window matches the time window in (b). (b) The waveforms of the stations near the uncatalogued event, time aligned to the origin time of the uncatalogued event (121.17 s after the Mw 7.8 mainshock), sorted by the distance from the uncatalogued event. For clarity, waveforms are filtered within the 5–50 Hz range to eliminate low-frequency signals from the distant Mw 7.8 mainshock. The blue dashed line with dots in (a) indicates the P-wave arrival times of the Mw 7.8 mainshock predicted based on a local 1D velocity model (Melgar et al., 2020) (Table S1 in Supporting Information S1), while red dashed lines with dots represent the S-wave arrival times. Blue dashed lines in (a, b) indicate the manually picked P-wave arrival times of the uncatalogued event, while red lines represent the S-wave arrival times.

analysis, the future availability of DAS recordings for cataloged events would allow us to measure the magnitude of an earthquake using DAS data, as shown in Yin et al. (2023).

4. Discussion

Using the seismic recordings on DAS and conventional seismometers, we successfully detected, located, and determined the magnitude of this uncatalogued M5.1 event. To illustrate how the new findings of this study contribute to our understanding of earthquake physics, we thoroughly discuss the physical triggering mechanism between the M7.8 mainshock and the M5.1 earthquake, as well as the potential nucleation phase of the M5.1 event, in subsequent subsections. Additionally, we summarize our conclusions and highlight DAS's potential in the detection and analysis of earthquake triggering. The future integration of innovative sensing technologies like

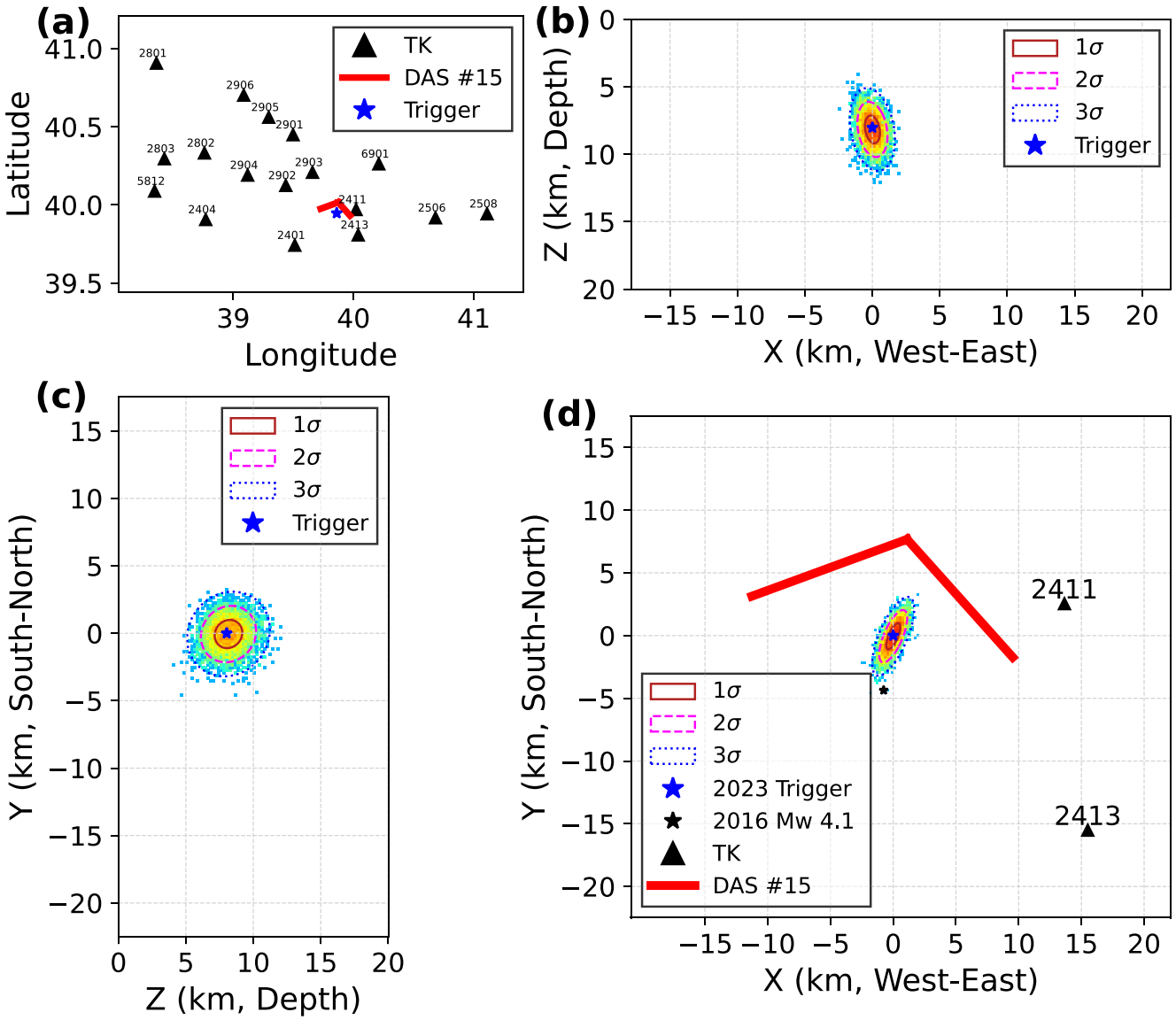

Figure 5. Location of the uncatalogued event (Latitude: 39.947°, Longitude: 39.860°, Depth: 8.02 km, 392 km away from the Mw 7.8 mainshock). (a) The map of stations with phase arrivals and DAS segment #15 utilized in locating the uncatalogued event. An enlarged 3-D view around the uncatalogued event is shown in (b–d). (b) The posterior probability density function and the optimal earthquake hypocenter in the X (longitude)—Z (depth) view. (c) Similar to (b) but in the Z (depth)—Y (latitude) view. (d) Similar to (b) but in the X (longitude)—Y (latitude) view. Contours labeled 1–3 σ in panels (b, c) represent one to three times the standard deviation. Note the precise locations of the DAS channels have been intentionally blurred due to security concerns.

DAS with existing seismic networks promises to enhance observations and deepen our knowledge of tectonics and earthquake physics.

4.1. Earthquake Triggering Mechanism

Investigating the mechanisms underlying earthquake triggering can provide crucial insights into the physical interactions between dynamics on different faults. To investigate if this M5.1 earthquake was triggered by the earlier Mw 7.8 mainshock, we calculate both the static and dynamic stress changes from the Mw 7.8 mainshock at the location of the M5.1 event. First, we calculate the static Coulomb stress changes using the USGS finite fault model via the Coulomb 3 package (Toda et al., 2011). The receiver fault is set to the depth of the uncatalogued event (8 km). The receiver fault orientation is inferred from the AFAD focal mechanism solution (strike: 192°, dip: 90°, rake: −33°) for the 2016 M4.1 earthquake, located only 4.4 km from the uncatalogued event (Figure 5d).

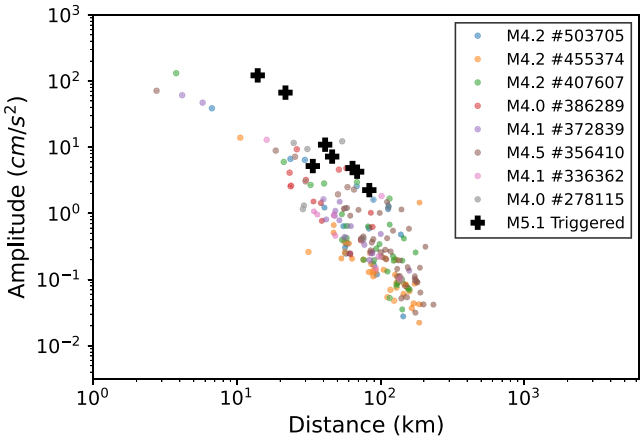

Figure 6. The distribution of peak amplitudes against corresponding epicentral distances for the uncatalogued M5.1 event and nearby cataloged events with Mw > 4. The # numbers in the legend are the event IDs in the AFAD catalog.

The focal mechanism solution of the 2016 M4.1 event matches the orientation of local faults in the map (Bozkurt, 2001). Figure 7a shows that the static Coulomb stress change is 0.013 MPa. Next, the peak dynamic stress change (σ) is calculated based on the peak ground velocity (PGV):

$$\sigma = \frac{\mu\,(\mathrm{PGV})}{c} \tag{2}$$

where μ is the shear modulus assigned as 35 GPa in this study (C. Li et al., 2023), and c is phase velocity assigned as 3.5 km/s in this study. The PGV at the station nearest to the uncatalogued event (TK2411) is 11.356 cm/s. The corresponding peak dynamic stress change is 1.136 MPa (Figure 7b), as expected significantly surpassing the static stress change of 0.013 MPa.

Both the static stress change (0.013 MPa) and the peak dynamic stress change (1.136 MPa) show positive values at the location of the M5.1 (Figure 7), indicating that both static and dynamic stress changes could be the triggering agents. However, the M5.1 event is more likely triggered by the dynamic stress change from the passing wave rather than the static stress change from the permanent fault displacement caused by the Mw 7.8 mainshock for the following reasons. First, our calculations show that the dynamic stress change at the nearest station is significantly larger (compare 1.136 MPa at station TK2411 and 0.013 MPa) than the static stress change (Figure 7). Even when considering the PGV of a lowpass filtered signal or values from other nearby stations, which could be slightly lower than the broadband PGV at the closest station, the peak dynamic stress change remains notably higher (e.g., compare 0.66 MPa at station TK2413 and 0.013 MPa) than the static stress change. This disparity can be attributed to the faster decrease in static stress change as moving away from the mainshock epicenter compared to the dynamic stress change (Freed, 2005). This holds true even though the triggered event is only one fault length away from the mainshock, a distance (392 km) that's shorter than typical remote dynamic triggering instances (Fan & Shearer, 2016; Hill & Prejean, 2015; Kilb et al., 2000). Second, the triggering time (121s post-mainshock) coincides with the passage of the mainshock's large amplitude S and surface waves, indicating instantaneous triggering (Figure 8a). Lastly, the triggered event occurred on a splay fault in the Northeast Anatolian Fault Zone near the North Anatolian Fault Zone (Figures 1 and 7) (Bozkurt, 2001; Irmak et al., 2012; Şengör et al., 1985). The Northeast Anatolian Fault Zone is distant and not directly connected to the East Anatolian Fault Zone where the M7.8 mainshock and its aftershocks occurred. It is noteworthy that the last $M \geq 5$ earthquake was in 1995 and the last $M \geq 7$ earthquake was in 1992 before this triggered event in the nearby 0.5-degree region based on the local AFAD catalog. These findings suggest that dynamic triggering is more likely than static triggering, and the fact that the M5.1 occurred within the wavetrain of the Mw 7.8 event suggests a causal triggering relationship.

4.2. Precursory Signals From Earthquake Nucleation or Nearby Events?

Beyond the triggering mechanism (Felzer & Brodsky, 2006; Richards-Dinger et al., 2010), the detailed physical nucleation process of earthquakes is another unsettled puzzle in seismology. For example, there is a long debate between the "cascade" model and the "preslip" model for earthquake nucleation (Gomberg, 2018; McLaskey, 2019). Observational evidence for the earthquake precursory signal is limited but can provide valuable insights into the physics of earthquake nucleation and hint at the earthquake's occurrence (Ellsworth & Beroza, 1995; Iio, 1995; Kilb & Gomberg, 1999; Mori & Kanamori, 1996; Tape et al., 2018). Tape et al. (2013) reported a 24 s exponential foreshock signal preceding the P arrivals of a dynamically triggered earthquake in Alaska supporting the "preslip" model (Tape et al., 2018). Previous studies identified a 44-min-long foreshock sequence preceding the 1999 Mw 7.6 Turkey earthquake (Özalaybey et al., 2002). Bouchon et al. (2011) first interpreted this sequence as repeating earthquakes, driven by the slow slip in the nucleation phase of the mainshock ("preslip" model). Conversely, Ellsworth and Bulut (2018) re-evaluated this sequence, proposing it might be better explained as a series of foreshocks triggering the mainshock ("cascade" model).

Prompted by these interesting observations in previous studies, we explored potential foreshocks or the nucleation phase of the M5.1 earthquake reported in this study. Interestingly, we identified clear signals lasting at least 5 seconds before the P arrivals of this event at the nearby stations (e.g., station TK2411 at 14 km and station

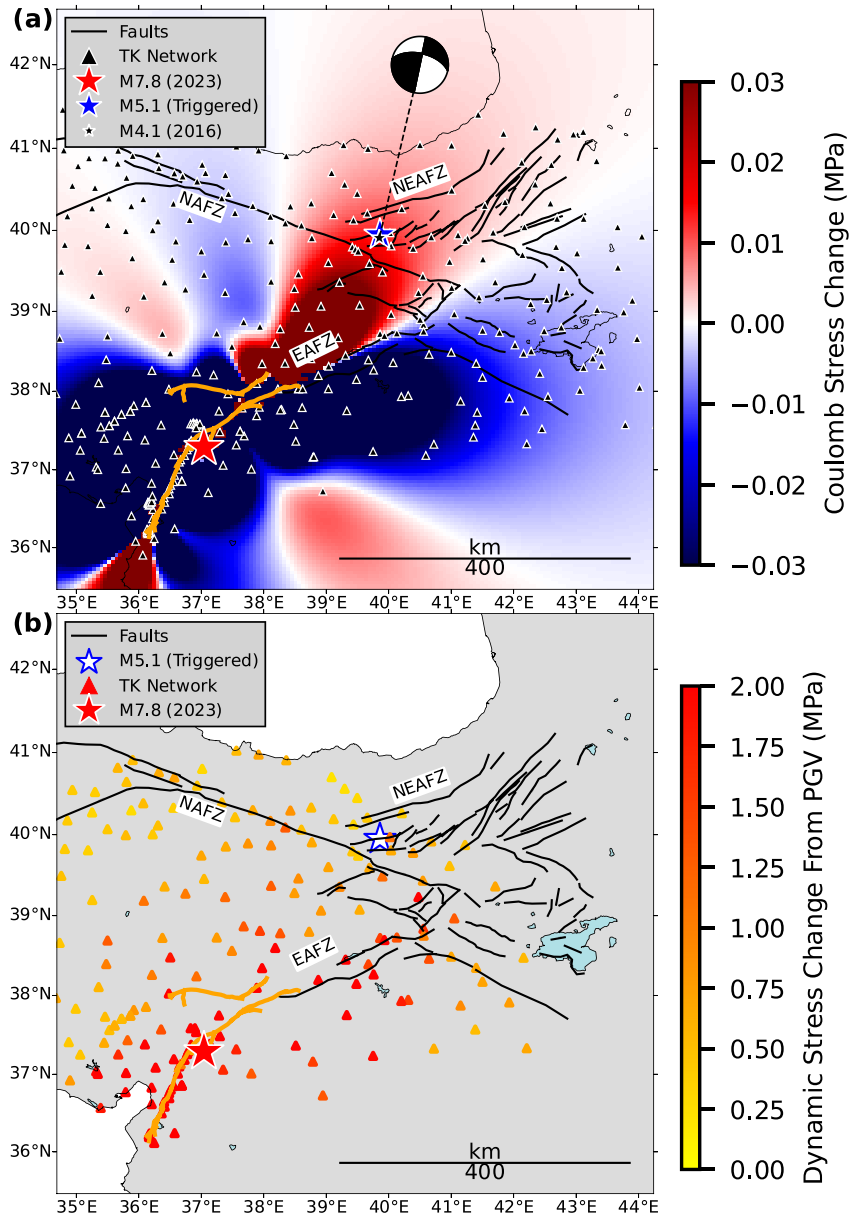

Figure 7. Mapping of the static and dynamic stress changes generated by the Mw 7.8 mainshock. (a) Static Coulomb stress change at the hypocenter of the triggered earthquake (blue star) is 0.013 MPa. (b) Dynamic stress change, inferred from PGV at the nearest station to the hypocenter of the triggered earthquake (blue star), is 1.136 MPa. Note the color scales are saturated at a maximum absolute stress change of 0.03 MPa in (a) and 2 MPa in (b) for plotting purposes to clearly show values near the triggered event, which is located 392 km from the M7.8 mainshock.

TK2413 at 22 km as shown in Figure 8). The signal is optimally visualized via a logarithmically scaled plot of the waveform's envelope (Figure 8c) (Tape et al., 2013). To negate potential confounding factors (e.g., underground structure along the ray path), Figure 8c compares the high-frequency envelope of the waveform recorded at the closest station (TK211) for both the 2023 M5.1 event and the 2016 M4.1 comparison event, which is close to the M5.1 event (Figure 5d). The 2016 M4.1 event occurred 4.4 km laterally and 6.0 km deeper relative to the 2023 M5.1 uncatalogued event. The patterns of the two time series are similar after the P arrivals ($t > 0$), but obviously different before the P arrivals ($t < 0$). To estimate the location of the possible foreshock signal, we investigate the amplitude's decay pattern with respect to the distance from the M5.1 event's epicenter (Figure 9). We observe complex relationships between amplitude and distance that don't conform to a straightforward decay pattern. Similarly, both the first arrivals and peak arrivals exhibit inconsistent delay patterns relative to the distance.

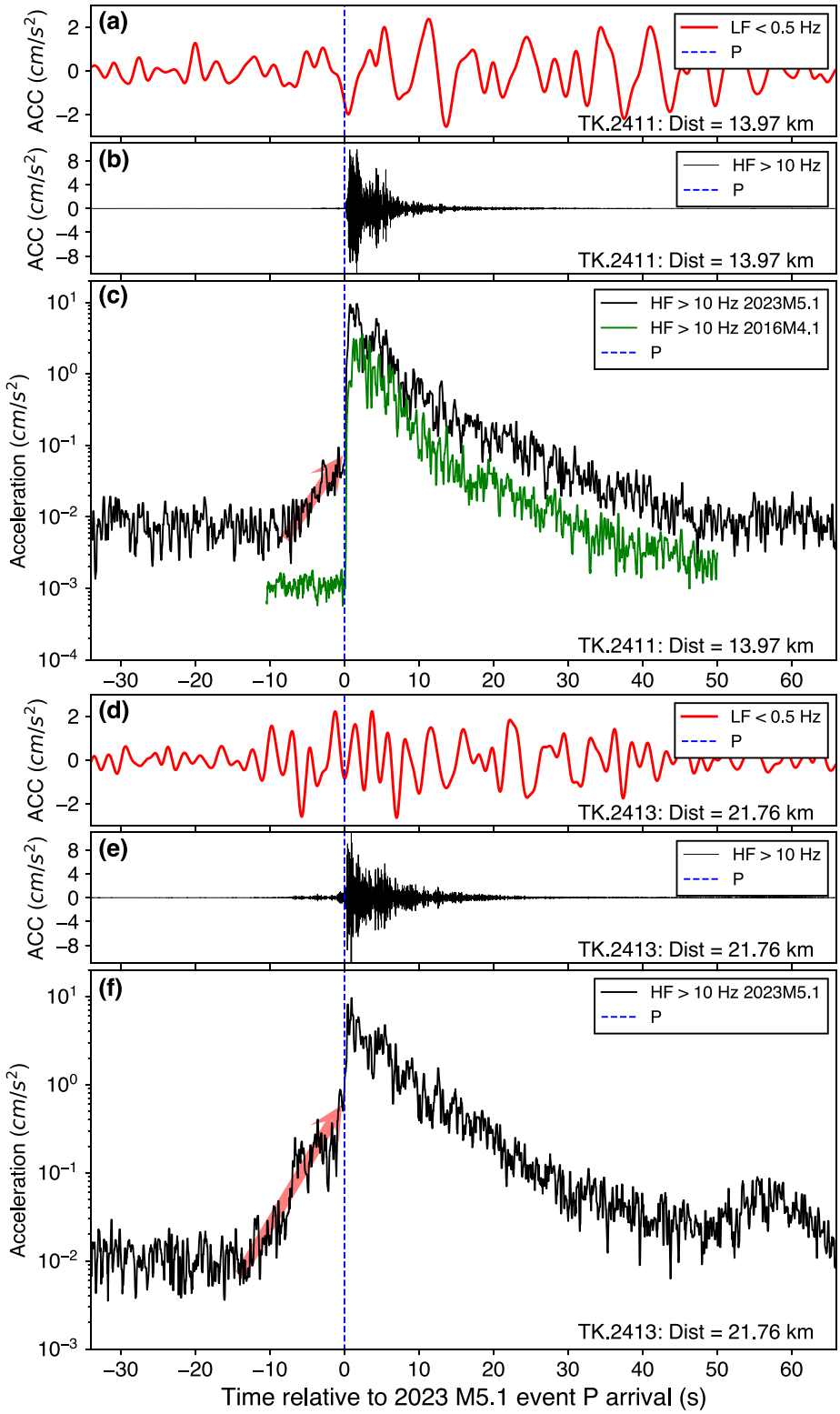

Figure 8.

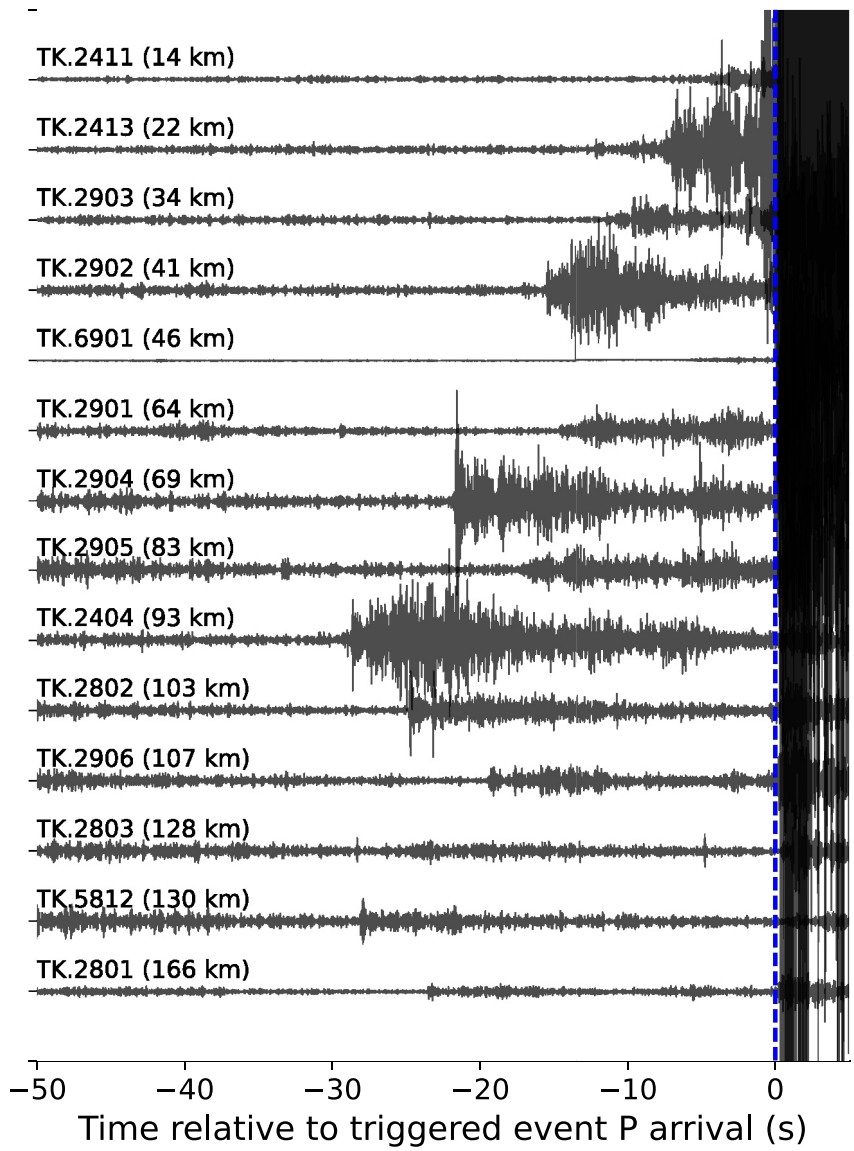

Figure 9. The signal preceding the P arrival of the M5.1 earthquake. Waveforms are the acceleration on the vertical component, filtered within the 10–50 Hz range (Figures S5 and S6 in Supporting Information S1), ordered by distance (label on the left) from the epicenter of the M5.1 earthquake, and aligned with its P arrival of the M5.1 earthquake. The blue vertical dashed line at $T = 0$s marks the P arrivals. The relative amplitude ratio across stations reflects the accurate physical amplitude ratio.

While the precursory signals preceding the P arrivals of the M5.1 earthquake on the two nearest stations (Figure 8) resemble observations from the 2012 dynamically triggered earthquake in Alaska (Tape et al., 2013), we think they are the signals from one or more separate, uncatalogued, smaller events triggered by the Mw 7.8 mainshock, rather than the nucleation phase of the M5.1 event (Tape et al., 2013). This is because we did not observe the amplitude decay and arrival time delay with distance, as demonstrated in the 2012 Alaska case (Tape et al., 2013). Therefore, we estimate the foreshock signal location to be at least 14 km away from the 2023 M5.1 Turkey

Figure 8. The signal preceding P arrivals of the 2023 M5.1 event on the two nearest stations. (a) The low-frequency (LF) signal from the distant Mw 7.8 mainshock on the TK2411 station. (b) The high-frequency (HF) signal from the local M5.1 earthquake on the TK2411 station. (c) The logarithmically scaled plot of the high-frequency (HF) waveform's envelope of the 2023 M5.1 earthquake and the 2016 M4.1 comparison event which is close to the M5.1 event (4.4 km apart, Figure 5d) on the TK2411 station. The red arrow marks the exponential precursory signals before the P arrivals. (d–f) Are similar to (a–c) but on the TK2413 station. All the waveforms are aligned on the P arrival of the M5.1 earthquake at each station marked by the blue vertical dashed line at $t = 0$s.

earthquake epicenter (Figure 9). However, their estimation of the location of the foreshock signal is within 20 km of the 2012 Alaska earthquake epicenter. Hawthorne and Ampuero (2017) later relocated the foreshock signal of the 2012 Alaska earthquake to within 2 km of the mainshock using a phase coherence approach. It's worth noting that the closest station to the 2013 M5.1 Turkey earthquake is 14 km away, compared to 34 km for the Alaska earthquake, which limits spatial resolution in the Alaska studies. Besides the conventional seismometers, we also attempted to detect the potential foreshock signal on the DAS data. However, because it is an intensity-based DAS system with high-level noise and a lack of accurate phase information, the weak signal remained undetected even after channel stacking.

5. Conclusions

In this study, we identified an uncatalogued M5.1 earthquake in Northeast Turkey, occurring shortly after the 2023 Mw 7.8 earthquake in Southeast Turkey. Initially detected via a DAS system spanning over one thousand kilometers, this event was subsequently validated through local conventional seismometers, providing precise time, location, and magnitude. This M5.1 earthquake occurred 121 s after and 392 km distant from the Mw 7.8 mainshock. Considering the static and dynamic stress changes from the Mw 7.8 mainshock at the triggered event's location, along with time and location details, we conclude that this M5.1 event was likely dynamically triggered by the Mw 7.8 mainshock. This represents an instance of instantaneous triggering, as the M5.1 event occurred within the time window of the S and surface waves from the Mw 7.8 mainshock. Additionally, we observed intriguing precursory signals preceding its P arrivals on the nearby seismometers, interpreted as signals from other uncatalogued, smaller triggered events nearby.

Our findings also highlight the potential of DAS in detecting and performing detailed analyses of earthquake triggering. Furthermore, our results demonstrate that a DAS system, initially developed for industry applications, can contribute to scientific inquiry and address community concerns regarding natural hazards, simultaneously offering industries additional benefits. For instance, the timely discovery of a nearby $M > 5$ earthquake with comprehensive information can mitigate potential infrastructure damage and associated losses. DAS technology is advancing rapidly, promising the emergence of more high-quality, quantitative DAS systems that will cover broader regions worldwide for future comprehensive earthquake studies (Spica et al., 2023).

Conflict of Interest

The authors declare no conflicts of interest relevant to this study.

Data Availability Statement

The necessary data including phase arrivals, peak ground accelerations, and the earthquake catalog to reproduce the main results are publicly available at Zhai (2023). The seismic waveforms of the Turkish National Strong Motion Network (Disaster and Emergency Management Authority, 1973), which is operated by Turkey's Disaster and Emergency Management Authority (AFAD), are publicly available from the Engineering Strong Motion Database by ORFEUS (Luzi et al., 2020) at https://esm-db.eu/#/event/INT-20230206_0000008. The DAS data supporting this research can be accessed from Luna-OptaSense at https://www.optasense.com/real-time-pipeline-monitoring, with restrictions on necessary licenses and agreements, and are not accessible to the public due to international energy security concerns. The earthquake location is calculated using NonLinLoc (Lomax et al., 2000, 2014), publicly available under the LGPL GNU license at https://github.com/alomax/NonLinLoc. The static Coulomb stress changes are calculated using Coulomb version 3 (Toda et al., 2011), publicly available under the Coulomb license at https://www.usgs.gov/node/279387. All links were last accessed in August 2023.

Acknowledgments
We thank Victor Yartsev for his help in preparing the raw DAS data. The manuscript has been enriched by the insightful comments from an anonymous reviewer, Debi Kilb, and editor Rachel Abercrombie. Additionally, we extend our thanks to Zhigang Peng, Zhe Jia, Yan Yang, and Weiqiang Zhu for their constructive discussions. This study is supported by the United States National Science Foundation (NSF, Grant EAR-1848166), the United States Geological Survey (USGS, Grant G23AP00111), the Gordon and Betty Moore Foundation, and the Braun Trust.

References

Aiken, C., & Peng, Z. (2014). Dynamic triggering of microearthquakes in three geothermal/volcanic regions of California. *Journal of Geophysical Research: Solid Earth*, *119*(9), 6992–7009. https://doi.org/10.1002/2014JB011218

Ajo-Franklin, J. B., Dou, S., Lindsey, N. J., Monga, I., Tracy, C., Robertson, M., et al. (2019). Distributed acoustic sensing using dark fiber for near-surface characterization and broadband seismic event detection. *Scientific Reports*, *9*(1), 1328. https://doi.org/10.1038/s41598-018-36675-8

Ambraseys, N. N. (1970). Some characteristic features of the Anatolian fault zone. *Tectonophysics*, *9*(2), 143–165. https://doi.org/10.1016/0040-1951(70)90014-4

Antonioli, A., Belardinelli, M. E., Bizzarri, A., & Vogfjord, K. S. (2006). Evidence of instantaneous dynamic triggering during the seismic sequence of year 2000 in south Iceland. *Journal of Geophysical Research*, *111*(B3), B03302. https://doi.org/10.1029/2005JB003935

Barbot, S., Luo, H., Wang, T., Hamiel, Y., Piatibratova, O., Javed, M. T., et al. (2023). Slip distribution of the February 6, 2023 Mw 7.8 and Mw 7.6, Kahramanmaraş, Turkey earthquake sequence in the East Anatolian Fault Zone. *Seismica*, *2*(3). Article 3. https://doi.org/10.26443/seismica.v2i3.502

Bouchon, M., Karabulut, H., Aktar, M., Özalaybey, S., Schmittbuhl, J., & Bouin, M.-P. (2011). Extended nucleation of the 1999 Mw 7.6 Izmit earthquake. *Science*, *331*(6019), 877–880. https://doi.org/10.1126/science.1197341

Bozkurt, E. (2001). Neotectonics of Turkey—A synthesis. *Geodinamica Acta*, *14*(1–3), 3–30. https://doi.org/10.1080/09853111.2001.11432432

Brodsky, E. E., Karakostas, V., & Kanamori, H. (2000). A new observation of dynamically triggered regional seismicity: Earthquakes in Greece following the August 1999 Izmit, Turkey earthquake. *Geophysical Research Letters*, *27*(17), 2741–2744. https://doi.org/10.1029/2000GL011534

Brodsky, E. E., & van der Elst, N. J. (2014). The uses of dynamic earthquake triggering. *Annual Review of Earth and Planetary Sciences*, *42*(1), 317–339. https://doi.org/10.1146/annurev-earth-060313-054648

Chavarria, J. A., Ugueto, G., Oukaci, Y., & Laflame, L. (2022). Assessing single and multiwell fiber optic data for microseismic monitoring: An example from HFTS2. *Unconventional Resources Technology Conference*, 230–240. https://doi.org/10.15530/urtec-2022-3722235

Dal Zilio, L., & Ampuero, J.-P. (2023). Earthquake doublet in Turkey and Syria. *Communications Earth & Environment*, *4*(1), 71. Article 1. https://doi.org/10.1038/s43247-023-00747-z

Delouis, B., van den Ende, M., & Ampuero, J.-P. (2023). Kinematic rupture model of the February 6th 2023 Mw7. 8 Turkey earthquake from a large set of near-source strong motion records combined by GNSS offsets reveals intermittent supershear rupture. *Authorea Preprints*. https://doi.org/10.22541/essoar.168286647.71550161/v1

DeMets, C., Gordon, R. G., Argus, D., & Stein, S. (1990). Current plate motions. *Geophysical Journal International*, *101*(2), 425–478. https://doi.org/10.1111/j.1365-246X.1990.tb06579.x

Disaster and Emergency Management Authority. (1973). Turkish national strong motion network. [Dataset]. Department of Earthquake, Disaster and Emergency Management Authority. https://doi.org/10.7914/SN/TK

Duman, T. Y., & Emre, Ö. (2013). The East Anatolian Fault: Geometry, segmentation and jog characteristics. *Geological Society, London, Special Publications*, *372*(1), 495–529. https://doi.org/10.1144/SP372.14

Ellsworth, W. L., & Beroza, G. C. (1995). Seismic evidence for an earthquake nucleation phase. *Science*, *268*(5212), 851–855. https://doi.org/10.1126/science.268.5212.851

Ellsworth, W. L., & Bulut, F. (2018). Nucleation of the 1999 Izmit earthquake by a triggered cascade of foreshocks. *Nature Geoscience*, *11*(7), 531–535. Article 7. https://doi.org/10.1038/s41561-018-0145-1

Fan, W., & Shearer, P. M. (2016). Local near instantaneously dynamically triggered aftershocks of large earthquakes. *Science*, *353*(6304), 1133–1136. https://doi.org/10.1126/science.aag0013

Felzer, K. R., & Brodsky, E. E. (2006). Decay of aftershock density with distance indicates triggering by dynamic stress. *Nature*, *441*(7094), 735–738. https://doi.org/10.1038/nature04799

Freed, A. M. (2005). Earthquake triggering by static, dynamic, and postseismic stress transfer. *Annual Review of Earth and Planetary Sciences*, *33*(1), 335–367. https://doi.org/10.1146/annurev.earth.33.092203.122505

Gibbons, S. J., & Ringdal, F. (2006). The detection of low magnitude seismic events using array-based waveform correlation. *Geophysical Journal International*, *165*(1), 149–166. https://doi.org/10.1111/j.1365-246X.2006.02865.x

Gomberg, J. (2018). Unsettled earthquake nucleation. *Nature Geoscience*, *11*(7), 463–464. Article 7. https://doi.org/10.1038/s41561-018-0149-x

Hawthorne, J. C., & Ampuero, J.-P. (2017). A phase coherence approach to identifying co-located earthquakes and tremor. *Geophysical Journal International*, *209*(2), 623–642. https://doi.org/10.1093/gji/ggx012

Helmstetter, A., Kagan, Y. Y., & Jackson, D. D. (2006). Comparison of short-term and time-independent earthquake forecast models for Southern California. *Bulletin of the Seismological Society of America*, *96*(1), 90–106. https://doi.org/10.1785/0120050067

Hill, D. P., & Prejean, S. G. (2015). Dynamic triggering. In *Treatise on geophysics* (pp. 273–304). Elsevier.

Hill, D. P., Reasenberg, P. A., Michael, A., Arabaz, W. J., Beroza, G., Brumbaugh, D., et al. (1993). Seismicity remotely triggered by the magnitude 7.3 Landers, California, earthquake. *Science*, *260*(5114), 1617–1623. https://doi.org/10.1126/science.260.5114.1617

Iio, Y. (1995). Observations of the slow initial phase generated by microearthquakes: Implications for earthquake nucleation and propagation. *Journal of Geophysical Research*, *100*(B8), 15333–15349. https://doi.org/10.1029/95JB01150

Irmak, T. S., Doğan, B., & Karakaş, A. (2012). Source mechanism of the 23 October, 2011, Van (Turkey) earthquake (Mw = 7.1) and aftershocks with its tectonic implications. *Earth Planets and Space*, *64*(11), 991–1003. Article 11. https://doi.org/10.5047/eps.2012.05.002

Ishii, M., Shearer, P. M., Houston, H., & Vidale, J. E. (2005). Extent, duration and speed of the 2004 Sumatra-Andaman earthquake imaged by the Hi-Net array. *Nature*, *435*(7044), 933–936. https://doi.org/10.1038/nature03675

Jaeger, J. C., Cook, N. G. W., & Zimmerman, R. (2009). *Fundamentals of rock mechanics*. John Wiley & Sons.

Jia, Z., Jin, Z., Marchandon, M., Ulrich, T., Gabriel, A.-A., Fan, W., et al. (2023). The complex dynamics of the 2023 Kahramanmaraş, Turkey, Mw 7.8-7.7 earthquake doublet. *Science*, *0*(0), eadi0685. https://doi.org/10.1126/science.adi0685

Kadirioğlu, F. T., Kartal, R. F., Kılıç, T., Kalafat, D., Duman, T. Y., Eroğlu Azak, T., et al. (2018). An improved earthquake catalogue (M ≥ 4.0) for Turkey and its near vicinity (1900–2012). *Bulletin of Earthquake Engineering*, *16*(8), 3317–3338. https://doi.org/10.1007/s10518-016-0064-8

Karrenbach, M., Ridge, A., Cole, S., Boone, K., Kahn, D., Rich, J., et al. (2017). DAS microseismic monitoring and integration with strain measurements in hydraulic fracture profiling. *Unconventional Resources Technology Conference*, 1316–1330. https://doi.org/10.15530/URTEC-2017-2670716

Kato, A., Nakamura, K., & Hiyama, Y. (2016). The 2016 Kumamoto earthquake sequence. *Proceedings of the Japan Academy, Series B*, *92*(8), 358–371. https://doi.org/10.2183/pjab.92.359

Kilb, D., & Gomberg, J. (1999). The initial subevent of the 1994 Northridge, California, earthquake: Is earthquake size predictable? *Journal of Seismology*, *3*(4), 409–420. https://doi.org/10.1023/A:1009890329925

Kilb, D., Gomberg, J., & Bodin, P. (2000). Triggering of earthquake aftershocks by dynamic stresses. *Nature*, *408*(6812), 570–574. Article 6812. https://doi.org/10.1038/35046046

Li, C., Peng, Z., Chaput, J. A., Walter, J. I., & Aster, R. C. (2021). Remote triggering of Icequakes at Mt. Erebus, Antarctica by large teleseismic earthquakes. *Seismological Research Letters*, *92*(5), 2866–2875. https://doi.org/10.1785/0220210027

Li, C., Peng, Z., Yao, D., Meng, X., & Zhai, Q. (2023). Temporal changes of seismicity in Salton Sea Geothermal Field due to distant earthquakes and geothermal productions. *Geophysical Journal International*, *232*(1), 287–299. https://doi.org/10.1093/gji/ggac324

Li, J., Kim, T., Lapusta, N., Biondi, E., & Zhan, Z. (2023). The break of earthquake asperities imaged by distributed acoustic sensing. *Nature*, *620*(7975), 1–7. https://doi.org/10.1038/s41586-023-06227-w

Li, J., Zhu, W., Biondi, E., & Zhan, Z. (2023). Earthquake focal mechanisms with distributed acoustic sensing. *Nature Communications*, *14*(1), 4181. Article 1. https://doi.org/10.1038/s41467-023-39639-3

Li, Z. F., Shen, Z. C., Yang, Y., Williams, E., Wang, X., & Zhan, Z. W. (2021). Rapid response to the 2019 Ridgecrest earthquake with distributed acoustic sensing. *AGU Advances*, *2*(2). https://doi.org/10.1029/2021AV000395

Lindsey, N. J., Dawe, T. C., & Ajo-Franklin, J. B. (2019). Illuminating seafloor faults and ocean dynamics with dark fiber distributed acoustic sensing. *Science*, *366*(6469), 1103–1107. https://doi.org/10.1126/science.aay5881

Lindsey, N. J., & Martin, E. R. (2021). Fiber-optic seismology. *Annual Review of Earth and Planetary Sciences*, *49*(1), 309–336. https://doi.org/10.1146/10.1146/annurev-earth-072420-065213

Lindsey, N. J., Martin, E. R., Dreger, D. S., Freifeld, B., Cole, S., James, S. R., et al. (2017). Fiber-optic network observations of earthquake wavefields. *Geophysical Research Letters*, *44*(23), 11792–11799. https://doi.org/10.1002/2017GL075722

Lindsey, N. J., Rademacher, H., & Ajo-Franklin, J. B. (2020). On the broadband instrument response of fiber-optic DAS arrays. *Journal of Geophysical Research: Solid Earth*, *125*(2), e2019JB018145. https://doi.org/10.1029/2019jb018145

Liu, G. M., Li, C. Y., Peng, Z. G., Li, X. M., & Wu, J. (2017). Detecting remotely triggered microseismicity around Changbaishan Volcano following nuclear explosions in North Korea and large distant earthquakes around the world. *Geophysical Research Letters*, *44*(10), 4829–4838. https://doi.org/10.1002/2017gl072511

Lomax, A., Michelini, A., & Curtis, A. (2014). Earthquake location, direct, global-search methods. In R. A. Meyers (Ed.), *Encyclopedia of complexity and systems science* (pp. 1–33). Springer. https://doi.org/10.1007/978-3-642-27737-5_150-2

Lomax, A., Virieux, J., Volant, P., & Berge-Thierry, C. (2000). Probabilistic earthquake location in 3D and layered models. In C. H. Thurber & N. Rabinowitz (Eds.), *Advances in seismic event location* (pp. 101–134). Springer Netherlands. https://doi.org/10.1007/978-94-015-9536-0_5

Luzi, L., Lanzano, G., Felicetta, C., D'Amico, M., Russo, E., Sgobba, S., et al. (2020). *Engineering strong motion database (ESM) (version 2.0)* (Vol. 2). Istituto Nazionale Di Geofisica e Vulcanologia (INGV). https://doi.org/10.13127/ESM

Mai, P. M., Aspiotis, T., Aquib, T. A., Cano, E. V., Castro-Cruz, D., Espindola-Carmona, A., et al. (2023). The destructive earthquake doublet of 6 February 2023 in South-Central Türkiye and Northwestern Syria: Initial observations and analyses. *The Seismic Record*, *3*(2), 105–115. https://doi.org/10.1785/0320230007

Martin, E. R., Castillo, C. M., Cole, S., Sawasdee, P. S., Yuan, S., Clapp, R., et al. (2017). Seismic monitoring leveraging existing telecom infrastructure at the SDASA: Active, passive, and ambient-noise analysis. *The Leading Edge*, *36*(12), 1025–1031. https://doi.org/10.1190/tle36121025.1

Mateeva, A., Lopez, J., Potters, H., Mestayer, J., Cox, B., Kiyashchenko, D., et al. (2014). Distributed acoustic sensing for reservoir monitoring with vertical seismic profiling. *Geophysical Prospecting*, *62*(4), 679–692. https://doi.org/10.1111/1365-2478.12116

McLaskey, G. C. (2019). Earthquake initiation from laboratory observations and implications for foreshocks. *Journal of Geophysical Research: Solid Earth*, *124*(12), 12882–12904. https://doi.org/10.1029/2019jb018363

Melgar, D., Ganas, A., Taymaz, T., Valkaniotis, S., Crowell, B. W., Kapetanidis, V., et al. (2020). Rupture kinematics of 2020 January 24 Mw 6.7 Doğanyol-Sivrice, Turkey earthquake on the East Anatolian Fault Zone imaged by space geodesy. *Geophysical Journal International*, *223*(2), 862–874. https://doi.org/10.1093/gji/ggaa345

Melgar, D., Taymaz, T., Ganas, A., Crowell, B., Öcalan, T., Kahraman, M., et al. (2023). Sub- and super-shear ruptures during the 2023 Mw 7.8 and Mw 7.6 earthquake doublet in SE Türkiye. *Seismica*, *2*(3). Article 3. https://doi.org/10.26443/seismica.v2i3.387

Meng, J., Kusky, T., Mooney, W. D., Bozkurt, E., Bodur, M. N., & Wang, L. (2024). Surface deformations of the 6 February 2023 earthquake sequence, eastern Türkiye. *Science*, *383*(6680), 298–305. https://doi.org/10.1126/science.adj3770

Molenaar, M. M., Hill, D., Webster, P., Fidan, E., & Birch, B. (2011). First downhole application of distributed acoustic sensing (DAS) for hydraulic fracturing monitoring and diagnostics. *SPE Hydraulic Fracturing Technology Conference*. https://doi.org/10.2118/140561-MS

Mori, J., & Kanamori, H. (1996). Initial rupture of earthquakes in the 1995 Ridgecrest, California sequence. *Geophysical Research Letters*, *23*(18), 2437–2440. https://doi.org/10.1029/96GL02491

Nayak, A., Ajo-Franklin, J., & the Imperial Valley Dark Fiber Team (2021). Distributed acoustic sensing using dark fiber for array detection of regional earthquakes. *Seismological Research Letters*, *92*(4), 2441–2452. https://doi.org/10.1785/0220200416

Okuwaki, R., Yagi, Y., Taymaz, T., & Hicks, S. P. (2023). Multi-scale rupture growth with alternating directions in a complex fault network during the 2023 South-Eastern Türkiye and Syria earthquake doublet. *Geophysical Research Letters*, *50*(12), e2023GL103480. https://doi.org/10.1029/2023GL103480

Özalaybey, S., Ergin, M., Aktar, M., Tapirdamaz, C., Biçmen, F., & Yörük, A. (2002). The 1999 İzmit earthquake sequence in Turkey: Seismological and tectonic aspects. *Bulletin of the Seismological Society of America*, *92*(1), 376–386. https://doi.org/10.1785/0120000838

Paitz, P., Edme, P., Graff, D., Walter, F., Doetsch, J., Chalari, A., et al. (2021). Empirical investigations of the instrument response for distributed acoustic sensing (DAS) across 17 Octaves. *Bulletin of the Seismological Society of America*, *111*(1), 1–10. https://doi.org/10.1785/0120200185

Parker, T., Shatalin, S., & Farhadiroushan, M. (2014). Distributed Acoustic Sensing–a new tool for seismic applications. *First Break*, *32*(2). https://doi.org/10.3997/1365-2397.2013034

Peng, Z., Hill, D. P., Shelly, D. R., & Aiken, C. (2010). Remotely triggered microearthquakes and tremor in central California following the 2010 Mw 8.8 Chile earthquake. *Geophysical Research Letters*, *37*(24), L24312. https://doi.org/10.1029/2010GL045462

Prejean, S. G., Hill, D. P., Brodsky, E. E., Hough, S. E., Johnston, M. J. S., Malone, S. D., et al. (2004). Remotely triggered seismicity on the United States West Coast following the Mw 7.9 Denali Fault earthquake. *Bulletin of the Seismological Society of America*, *94*(6B), S348–S359. https://doi.org/10.1785/0120040610

Reitman, N. G., Briggs, R., Barnhart, W. D., Jobe, J. A., DuRoss, C. B., Hatem, A. E., et al. (2023). Fault rupture mapping of the 6 February 2023 Kahramanmaraş, Türkiye, earthquake sequence from satellite data [Dataset]. U.S. Geological Survey. https://doi.org/10.5066/P985I7U2

Ren, C., Wang, Z., Taymaz, T., Hu, N., Luo, H., Zhao, Z., et al. (2024). Supershear triggering and cascading fault ruptures of the 2023 Kahramanmaraş, Türkiye, earthquake doublet. *Science*, *383*(6680), 305–311. https://doi.org/10.1126/science.adi1519

Richards-Dinger, K., Stein, R. S., & Toda, S. (2010). Decay of aftershock density with distance does not indicate triggering by dynamic stress. *Nature*, *467*(7315), 583–586. https://doi.org/10.1038/nature09402

Richter, C. F. (1935). An instrumental earthquake magnitude scale. *Bulletin of the Seismological Society of America*, *25*(1), 1–32. https://doi.org/10.1785/bssa0250010001

Scholz, C. H. (2019). *The mechanics of earthquakes and faulting*. Cambridge University Press.

Şengör, A., Görür, N., & Şaroğlu, F. (1985). Strike-slip faulting and related basin formation in zones of tectonic escape: Turkey as a case study.

Shelly, D. R., Beroza, G. C., & Ide, S. (2007). Non-volcanic tremor and low-frequency earthquake swarms. *Nature*, *446*(7133), 305–307. https://doi.org/10.1038/nature05666

Spica, Z. J., Ajo-Franklin, J., Beroza, G. C., Biondi, B., Cheng, F., Gaite, B., et al. (2023). PubDAS: A PUBlic distributed acoustic sensing datasets repository for geosciences. *Seismological Research Letters*, *94*(2A), 983–998. https://doi.org/10.1785/0220220279

Spica, Z. J., Perton, M., Martin, E. R., Beroza, G. C., & Biondi, B. (2020). Urban seismic site characterization by fiber-optic seismology. *Journal of Geophysical Research: Solid Earth*, *125*(3), e2019JB018656. https://doi.org/10.1029/2019JB018656

Tang, V., Seetharaman, P., Chao, K., Pardo, B. A., & van der Lee, S. (2020). Automating the detection of dynamically triggered earthquakes via a deep metric learning algorithm. *Seismological Research Letters*, *91*(2A), 901–912. https://doi.org/10.1785/0220190165

Tape, C., Holtkamp, S., Silwal, V., Hawthorne, J., Kaneko, Y., Ampuero, J. P., et al. (2018). Earthquake nucleation and fault slip complexity in the lower crust of central Alaska. *Nature Geoscience*, *11*(7), 536–541. Article 7. https://doi.org/10.1038/s41561-018-0144-2

Tape, C., West, M., Silwal, V., & Ruppert, N. (2013). Earthquake nucleation and triggering on an optimally oriented fault. *Earth and Planetary Science Letters*, *363*, 231–241. https://doi.org/10.1016/j.epsl.2012.11.060

Toda, S., Stein, R., Özbakir, A., Gonzalez-Huizar, H., Sevilgen, V., Lotto, G., & Sevilgen, S. (2023). Stress change calculations provide clues to aftershocks in 2023 Türkiye earthquakes. *Temblor*. https://doi.org/10.32858/temblor.295

Toda, S., Stein, R. S., Sevilgen, V., & Lin, J. (2011). *Coulomb 3.3 Graphic-rich deformation and stress-change software for earthquake, tectonic, and volcano research and teaching-user guide (Report 2011–1060; Open-File Report)*. USGS Publications Warehouse. https://doi.org/10.3133/ofr20111060

Walter, F., Gräff, D., Lindner, F., Paitz, P., Köpfli, M., Chmiel, M., & Fichtner, A. (2020). Distributed acoustic sensing of microseismic sources and wave propagation in glaciated terrain. *Nature Communications*, *11*(1), 2436. Article 1. https://doi.org/10.1038/s41467-020-15824-6

Williams, E. F., Fernández-Ruiz, M. R., Magalhaes, R., Vanthillo, R., Zhan, Z., González-Herráez, M., & Martins, H. F. (2019). Distributed sensing of microseisms and teleseisms with submarine dark fibers. *Nature Communications*, *10*(1), 5778. https://doi.org/10.1038/s41467-019-13262-7

Yao, D., Peng, Z., Kaneko, Y., Fry, B., & Meng, X. (2021). Dynamic triggering of earthquakes in the North Island of New Zealand following the 2016 Mw 7.8 Kaikōura earthquake. *Earth and Planetary Science Letters*, *557*, 116723. https://doi.org/10.1016/j.epsl.2020.116723

Yin, J., Zhu, W., Li, J., Biondi, E., Miao, Y., Spica, Z. J., et al. (2023). Earthquake magnitude with DAS: A transferable data-based scaling relation. *Geophysical Research Letters*, *50*(10), e2023GL103045. https://doi.org/10.1029/2023gl103045

Zhai, Q. (2023). Data of the uncatalogued magnitude-5 dynamically triggered event after the 2023 Turkey earthquake (version 1) [Dataset]. CaltechDATA. https://doi.org/10.22002/VZAW8-SH665

Zhai, Q., Peng, Z., Chuang, L. Y., Wu, Y.-M., Hsu, Y.-J., & Wdowinski, S. (2021). Investigating the impacts of a wet typhoon on microseismicity: A case study of the 2009 typhoon Morakot in Taiwan based on a template matching catalog. *Journal of Geophysical Research: Solid Earth*, *126*(12), e2021JB023026. https://doi.org/10.1029/2021jb023026

Zhai, Q., Peng, Z., Matsubara, M., Obara, K., & Wang, Y. (2023). Spatiotemporal variations of intermediate-depth earthquakes before and after 2011 Tohoku earthquake revealed by a template matching catalog. *Geophysical Research Letters*, *50*(22), e2023GL104068. https://doi.org/10.1029/2023GL104068

Zhan, Z. (2019). Distributed acoustic sensing turns fiber-optic cables into sensitive seismic antennas. *Seismological Research Letters*, *91*(1), 1–15. https://doi.org/10.1785/0220190112

Zhu, W., & Beroza, G. C. (2018). PhaseNet: A deep-neural-network-based seismic arrival time picking method. *Geophysical Journal International*. https://doi.org/10.1093/gji/ggy423

Zhu, W., Biondi, E., Li, J., Yin, J., Ross, Z. E., & Zhan, Z. (2023). Seismic arrival-time picking on distributed acoustic sensing data using semi-supervised learning. *Nature Communications*, *14*(1), 8192. Article 1. https://doi.org/10.1038/s41467-023-43355-3